Microporous and Mesoporous Materials 222 (2016) 9–22

Contents lists available at ScienceDirect

Microporous and Mesoporous Materials

journal homepage: www.elsevier.com/locate/micromeso

Exchanged lanthanum in InHMOR and its impact on the catalytic performance of InHMOR. Spectroscopic, volumetric and microscopic studies

Hernán P. Decolatti [a], Esteban G. Gioria [a], Santiago N. Ibarlín [a], Nuria Navascués [b], Silvia Irusta [b], Eduardo E. Miró [a], Laura B. Gutierrez [a, *]

[a] Instituto de Investigaciones en Catálisis y Petroquímica, INCAPE, (FIQ, UNL-CONICET), Santiago del Estero 2829, 3000 Santa Fe, Argentina
[b] Department of Chemical and Environmental Engineering, Institute of Nanoscience of Aragón (INA), University of Zaragoza, 50018 Zaragoza, Spain

ARTICLE INFO

Article history:
Received 26 June 2015
Received in revised form
16 September 2015
Accepted 24 September 2015
Available online 9 October 2015

Keywords:
Indium-mordenite
Lanthanum-mordenite
Dealumination
Zeolite hydrothermal stability
NO_x-SCR

ABSTRACT

The incorporation of lanthanum by ion exchange into InHMordenite was studied in order to investigate the modification of the physicochemical properties of the InHM catalysts. The prepared solids, LaInHM and InHM, were treated under rigorous reaction conditions, i.e. 25 h of TOS with addition of 10% of water and 500 °C. The structural changes of the catalysts were followed by spectroscopic, volumetric and microscopic studies. The presence of lanthanum in the InHM acts like a protection for the zeolite structure avoiding the formation of EFAl species, but the alteration of the indium environment into the matrix leads to a reduction of the catalytic yield of the InHM catalyst. In fact the XPS results revealed that the concentration of the indium active sites $(InO)^+$ in LaInHM is lower than in the InHM catalyst, while the remaining indium species interact strongly with Lanthanum. After the reaction, a decrease of In active site in the LaInHM catalyst was observed, suggesting a closer interaction In–La which was later corroborated by TEM microscopy. On the other hand, a steric factor between the side channels of the mordenite and the hydrated cation of La during the exchange process locates lanthanum in outer position, with the consequent loss of pore volume and area specific. The lanthanum exchanged ions protect the deactivation process by structure collapse, but negatively affect the activity of the InHM catalyst.

1. Introduction

It is well-known that zeolites as catalysts are complex materials formed by different components which give its characteristic properties to the zeolite. The different types of zeolitic structures together with the vast number of combinations of elements that can be associated to these matrices result in a vast array of catalysts that may be actives for many industrial reactions. The role of such components can be purely catalytic; they can act as stabilizing agents or just provide particular physical properties to the zeolitic support. For the catalytic goals the incorporation of active metals by different methods conduces to complex interactions between the guest components and the zeolitic matrix with the consequent improvement in the global catalytic performance of the modified zeolite. Nevertheless, in all cases the zeolitic catalysts undergo changes during its use under reaction conditions. The inside zeolite transformations can range from the loss of crystallinity, the migration of the metals from their original positions, the agglomeration of active particles sites, the changes on the strength and distribution of acid sites to pore blockage. By now, it is known that zeolites are not stable under rigorous conditions such as high temperature gas streams containing water, and it is for this reason that the use of zeolite-based catalysts is limited.

Many efforts have been made in order to explain the deactivation mechanisms of the technical relevant zeolites (MFI, MOR, FER, BEA, Y) [1,2], and to improve the durability of these materials. But drawing general conclusions is difficult, due to the extensive possibilities of combinations between structures, zeolite guest components (with different natures and contents), preparation methods, and conditions of the pretreatments and the reactions. These different combinations as regards materials and procedures conduce to different authors reaching to highly controversial findings when studying similar materials.

* Corresponding author. Tel./fax: +54 342 4536861.
E-mail address: lbgutier@fiq.unl.edu.ar (L.B. Gutierrez).

http://dx.doi.org/10.1016/j.micromeso.2015.09.042
1387-1811/

They all agree that exposure of zeolitic catalysts to water vapor at high temperatures irreversibly depresses the activity because some structural changes occur in the solids. Among them: (i) Dealumination, i.e., tetrahedral Al^{3+} ion removal from the zeolite lattice, (ii) Formation of metal oxides, loss of the dispersion and migration or sinterization of exchanged cations to highly coordinated non-accessible locations.

Several authors have studied zeolite deactivation in which the active site is the exchanged cobalt, but none of these studies evaluate the catalysts for more than 50 h on stream [3–8]. Towards further improvements, bimetallic catalysts were also proposed [9–15]. However, the durability of zeolite-based catalysts is not long enough yet to make its use economically feasible for industrial process.

Y zeolites are extensively used in the fluid catalytic cracking (FCC) of petroleum distillates so they have been exhaustively studied. It has been found that Rare Earth (RE) ions exchanged into the Y zeolite play an important role in the stabilization of such structure. These cations improve the acidity, the cracking activity, and the thermal stability [16,17]. A probable mechanism which may conduce to enhance the durability of these catalysts is the formation of lanthanum-hydroxyl species in zeolite channels, following thermally induced hydrolysis of the $[RE(H_2O)_n]^{3+}$ cations upon calcination [18] and their migration to smaller cages [19–23]. The thermal stability of HY zeolite is also improved by lanthanum exchange and to a lesser extent by cerium exchange. The reason is probably related to the increase in the ionic field within the crystal, but it cannot be solely explained by this effect. Thermal stability of LaHY catalyst is higher than cerium zeolites, fact that can be related to the particular properties of the rare earth cations, but it is difficult to establish what the relevant properties of the involved rare earth are [23].

On the other hand, the zeolites modified by the addition of La were studied by theoretical methods in order to corroborate the hydrothermal stability. In fact, Bao and co-workers [24,25] reported a density functional calculation (DFT) to the improvement in hydrothermal stability of La-modified ZSM-5. They investigate the location and binding of lanthanum cations, i.e., $La(OH)^{2+}$ on H-ZSM-5 and they found that the charges on both Al and O atoms in La-ZSM-5 show an increase compared to H-form zeolite, which would undoubtedly lead to a stronger mutual interaction and, hence, enhance the stability of the aluminum tetrahedron anion $[AlO_4]^-$. Moreover, $La(OH)^{2+}$ seems to have thickened the zeolite framework, which can effectively retard the process of dealumination. Yang et al. also studied by DFT the hydrothermal stabilities of different Metal/ZSM-5 zeolites and they concluded that the binding energies of the metal cations, which decreased as La/ZSM-5 > Ca/ZSM-5 > Mg/ZSM-5 > K/ZSM-5 > Rb/ZSM-5 > Na/ZSM-5 > Zn/ZSM-5 > H/ZSM-5, determined the relative hydrothermal stabilities of different metal exchanged ZSM-5 zeolites [26].

Additionally the high catalytic activity of zeolites modified with indium for the selective catalytic reduction (SCR) of NO_x with methane have been well-documented by several authors [27–33]. Different preparation methods of In-Zeolites (MOR, FER, ZSM-5) catalysts together with the addition of different co-cations were reported. Some of the bimetallic formulations yielded better results than monometallic catalysts but the reaction mechanism and the nature of the active sites became more complex. Therefore, the interaction between the species present in the zeolitic matrix became the focus of many research studies and significant progress has been achieved in this field [34–40]. However, the common point among all these authors' conclusions resulted that the ion $(InO)^+$ exchanged into the zeolitic matrix is the active site, while the co-cation may improve the catalytic performance. However the hydrothermal stability of In-zeolites has been hardly studied.

In this vein, the main aim of this work is to perform a detailed characterization study of La and In co-exchanged mordenite, in order to investigate both the La species generated into the zeolite matrix and their influence on the exchanged Indium. To achieve this aim XRD, pyridine desorption, XPS, FTIR and TEM techniques were applied in order to understand better both surface and bulk properties of the La,In mordenite samples. In addition, taking into account that In-zeolites are active and selective catalysts for the SCR of NO_x with CH_4, and that lanthanum could improve the stability of the mordenite structure [8], this reaction was performed to evaluate probably stabilizing properties as well as possible synergic effects between La and In in a similar way with the La,Co-Mordenite catalytic system [8]. Nevertheless, this study could be of interest to be applied in other catalytic reactions.

2. Experimental

2.1. Catalyst synthesis

The catalysts were prepared by ion exchange starting from Na-mordenite (NaM) (Zeolyst CBV 10A, Si/Al = 6.5). The ion exchanged form H-mordenite (HM) was prepared following the procedure reported by Gutierrez et al. [41]. The InHM catalyst containing 0.5 wt% of indium was prepared by wet impregnation conventional method with $In(NO_3)_3$ on HM support. Then the InHM solid was pretreated by the following steps: (i) heating in air flow at 500 °C for 10 h, (ii) reduction at 500 °C for 2 h with pure hydrogen and (iii) calcination with pure O_2 at 500 °C for 2 h. After each step the solid was flushed with pure He for 30 min.

Aliquots of HM and InHM were contacted with a $La(NO_3)_3$ aqueous solution during 36 h at RT for ion exchange of La and finally LaHM and LaInHM solids were obtained. All La-containing catalysts were treated in flowing oxygen for 10 h at 500 °C. Table 1 shows the composition of the prepared catalyst.

2.2. Catalyst characterization

2.2.1. Elements quantification

Atomic concentrations in the solid materials were determined by inductively coupled plasma atomic emission spectroscopy (ICP-OES). The measurements were performed in a Perkin Elmer Optima 2100 DV. Samples were dissolved using a mixture of perchloric and nitric acids.

2.2.2. X-ray photoelectron spectroscopy (XPS)

The X-ray Photoelectron analysis (XPS) was performed with an Axis Ultra DLD (Kratos Tech.). The spectra were excited by the monochromatized AlKα source (1486.6 eV) run at 15 kV and 10 mA. For the individual peak regions, pass energy of 20 eV was used. Survey spectrum was measured at 160 eV pass energy.

Table 1
Compositions of the synthesized catalysts.

Catalyst	In (wt%)[a]	La (wt%)[a]	%IE[b]	La/In[c]
LaHM	–	1.85	14.6	–
InHM	0.5	–	2.3	–
LaInHM	0.5	0.96	9.8	0.63

[a] Analyzed using inductively coupled plasma technique (ICP).
[b] Ion exchange rate (%IE) assuming that a stoichiometric exchange process take place with 3 monovalent ammonium ions being replaced by one $La(OH)^{2+}$ ion and one monovalent $(InO)^+$ ion.
[c] Atomic ratio.

Analyses of the peaks were performed with the CasaXPS software, using a weighted sum of Lorentzian and Gaussian components curves after Shirley background subtraction. The binding energies were referenced to the internal C 1s (284.9 eV) standard. The relative atomic concentration between elements was calculated from their respective main core-level components with spectrometer atomic sensitive factors and after background subtraction.

2.2.3. X-ray diffraction (XRD)

The XRD patterns of the fresh and used solids were obtained with an XD-D1 Shimadzu instrument with a monochromator, CuK_α radiation and operated at 35 kV and 40 mA. The scan rate was $1^\circ.min^{-1}$ for the 2θ range of 5° to 50°.

2.2.4. BET area and pore volume

Nitrogen adsorption isotherms were measured at liquid-nitrogen temperature (77 K) and at a relative pressure (P/P_0) interval between 6×10^{-7} and 0.998 in an automated Quantachrome sorptometer. The catalyst samples were outgassed prior to measurements at 300 °C overnight under a pressure of 10^{-5} Pa. The BET model was used in the relative pressure range 0.01–0.10 to estimate the total surface area, while the pore volume was calculated from the saturation N_2 adsorption capacity of the zeolite micropores.

2.2.5. Temperature programmed desorption of pyridine (Py-TPD)

Pyridine TPD experiments were carried out to evaluate the acid site types of the samples. The catalysts were pre-treated in situ in N_2 flow at 300 °C during 1 h. After cooling down to room temperature, three consecutive saturation steps with pure pyridine were performed. Then, pure nitrogen was flowed and the temperature was increased up to 150 °C, until no physisorbed pyridine was detected. The TPD experiments were carried out by heating at 12 °C min^{-1} in the temperature range 150–750 °C. The gases coming out of the analysis cell passed through a methanation reactor loaded with a Ni-based catalyst. The desorbed pyridine was converted into methane with a H_2 stream which was continuously measured using a FID detector. Finally the methane production was directly related with the desorbed pyridine.

2.2.6. FTIR and CO adsorption

The samples were prepared by compressing the solids at 4.10 Pa in order to obtain self-supporting pellets. They were mounted on a transportable infrared cell with CaF_2 windows and with an external oven. The pretreatment was performed in a high vacuum system. The samples were first outgassed at 400 °C for 12 h in a dynamic vacuum of 1.3×10^{-4} Pa. Then, they were cooled to room temperature and CO was introduced into the cell controlling the CO pressure at ca. 5, 50 and 100 Torr.

2.2.7. TEM specifications

Prepared catalysts were analyzed by Transmission Electron Microscopy (TEM). The samples for TEM analysis were prepared by re-suspending the corresponding sample in ethanol, dropping the suspension onto a 200 mesh carbon-coated copper grid (Electron Microscopy Sciences) and letting it dry under ambient air with the aid of anti-capillary tweezers. TEM and EDX measures were performed in a HR Tecnai F30, FEI.

2.3. Catalytic tests

The catalyst powders were tested in a flow-through reactor with controlled gas flow and heating. The reactant stream composition was: 1000 ppm CH_4, 1000 ppm NO and 2% O_2 in He (GHSV: 7500 h^{-1}). The reactor effluents were monitored for CH_4, CO, NO, N_2O and NO_2 quantification using an FTIR spectrometer (Thermo Mattson Genesis II) equipped with a gas cell with CaF_2 windows. One hundred and fifty scans were collected with a nominal resolution of 1 cm^{-1} and averaged to get a spectrum. The CH_4 to CO_2 and the NO_x to N_2 conversions were defined as $C_{NOx}(\%) = (1 - [NO_x]/[NO_x]^0) * 100$, and $C_{CH4}(\%) = (1 - [CH_4]/[CH_4]^0) * 100$, where $[NOx]^0$ and $[CH_4]^0$ stand for the NO and CH_4 concentration in the feed, respectively. The concentration of N_2 was determined from the nitrogen balance.

For the stability studies, 10% of water was added by flowing the reactant stream through a saturator after the initial dry test. All catalysts were kept on stream for 25 h at 500 °C under these conditions; the conversion was measured periodically.

3. Results and discussion

3.1. Catalytic activity

The maximum conversion reached with the InHM catalyst under dry conditions resulted 75% at 400 °C, while with LaInHM 48% at 450 °C. This means that the incorporation of lanthanum do not improve the catalytic activity of the InHM solids.

As the main goal of this work is to evaluate the probably stabilizing properties of exchanged lanthanum into InHM, the comparison of the hydrothermal stability between InHM and LaInHM was performed by measuring the catalytic activity under rigorous conditions: addition of 10% H_2O at 500 °C and TOS 25 h. After 25 h under reaction, the loss of activity of the InHM catalyst was 16% while in the LaInHM resulted 76%.

The catalytic activity results at 500 °C are reported in Table 2. That table shows that the initial NO to N_2 conversion (0% H_2O) with the LaInHM was higher than the conversion obtained with InHM, and the selectivity followed the inverse trend. When 10% of water was added to the reaction stream the LaInHM catalyst showed a significant sensibility to the presence of water. In fact as soon as water was added the conversion on this catalyst decreased 73% in contrast to the InHM solid in which the NO to N_2 conversion dropped down only 16%. After 25 h time on wet stream (500 °C) the final conversion with InHM was 13% lower than the initial conversion, while the LaInHM solid ended with a conversion 67% lower than the initial value (0% H_2O). The evaluation of the NO and CH_4 conversions along the TOS is shown in the attached Supplementary data. The negligible activity of LaHM solid for this reaction was previously reported by Gutierrez and Lombardo [8].

The catalytic response of catalyst with La as co-cation into the InH-mordenite resulted differently from the observed by Gutierrez and Lombardo for CoH-MOR [8]. From the basis that indium and cobalt behave differently into the same matrix it would not be wrong to assume that the presence of La can conduce to different specific changes in the InHM catalyst compare to the CoLaHM solid. In fact it can be noted that La does not improve greatly the hydrothermal stability of the InHM catalyst. The $(InO)^+$ species into the zeolites have been found to be the active sites for the NO-SCR with methane, but their catalytic properties highly depend on the coordination environment into the zeolitic matrix. On the other hand, the commonly present InO_x species enhance the methane oxidation, resulting in the increase of methane total oxidation and consequently the loss of selectivity [30,34–36]. However, there are not reports which study the hydrothermal stability of In-zeolite catalysts for long TOS.

Therefore, with these reported pieces of evidence and the results obtained in this work, it has resulted of interest to make a characterization of the In–La–Mordenite catalysts in order to explain the effects of La–In interaction into the mordenite and the impact of the reaction on the structure of the catalysts.

Table 2
Stability study of the prepared catalysts for the SCR of NO with CH_4 at 500 °C and TOS 0 h and 25 h.[a]

Catalyst	Selectivity, S_{N_2} (%) NO_x conversion, X_{NO} (%)							
	0% H_2O, 0 h		10% H_2O 0 h		0% H_2O, 25 h		10% H_2O 25 h	
	S_{N_2}(%)[b]	X_{NO}(%)	S_{N_2}(%)[b]	X_{NO}(%)	S_{N_2}(%)[b]	X_{NO}(%)	S_{N_2}(%)[b]	X_{NO}(%)
InHM	45	31	18	26	19	34	20	27 (16%)
LaInHM	32	45	23	12	12	35	24	15 (76%)

[a] Reaction conditions: GHSV = 7500 h^{-1}, [NO] = [CH_4] = 1000 ppm, [O_2] = 2%, [H_2O] = 10%, T = 500 °C.
[b] S_{N_2} (%): Selectivity to N_2, S_{N_2} (%) = X_{NO}/X_{CH_4}*50, in brackets the total lose of conversion from the initial value.

3.2. XPS results

In Table 3 the binding energies (BE) for La $3d_{5/2}$ and In $3d_{5/2}$ together with atomic ratios of the main elements of the synthesized catalysts are presented. The In spectrum for fresh InHM solid presents just one peak at 446.4 eV that can be associated with species that interact strongly with the zeolite (exchanged $(InO)^+$ and/or In_xO_y) [42]. On the one hand, for the used solid the fitting of the In $3d_{5/2}$ peak could be done only by considering two signals. The first one at low BE (444.2 eV) could be associated to bulk In_2O_3 [43] and the second signal at 445.9 eV could be also associated with exchanged $(InO)^+$ and/or In_xO_y species or to isolated oxyindium species [43]. In solids containing lanthanum (fresh and used) the component at higher BE (446.2–446.3 eV) as for the InHM solid can also be related also to the presence of $(InO)^+$ and/or In_xO_y species [43]. In 3d signals at low BE (445.0 eV) were previously ascribed to In(I) cations in solids prepared by a dry technique based on the use of $InCl_3$ sublimation [30]. More recently in In/zeolites prepared by reductive solid-state ion exchange the peak at 445.4 eV was assigned to the presence of isolated In^+ cations bounded to zeolite-bridged framework [43]. On the other hand, for solids prepared by aqueous ion exchange only, intrazeolite In oxo species were previously observed [30]. Schmidt et al. [34] suggest that intra-zeolite In can be obtained by ion exchange, but only to a low extent and with enrichment of the indium in the external zeolite layers. Besides, it is known that In^+ cations are not stable in air [44]. In view of the literature the presence of In(I) should be ruled out in the prepared LaInHM solids. The peak at 454.2–454.3 eV could be related to indium oxidized species ($(InO)^+$ and/or In_xO_y) interacting with the higher charge density of La^{3+} [45] as was found in La doped indium oxide.

The La $3d_{5/2}$ BE in the fresh catalyst was 836.8 eV, higher than the values reported for $La_2O_2CO_3$ (835.0 eV) [8] and for La_2O_3 (834.9 eV) [46]. The BE shift between La 3d peaks in the bulk oxide and the zeolite framework was assigned to La ions highly dispersed in the zeolite lattice that would be coordinated by H_2O molecules and by oxygen engaged in the partially covalent bonding of the zeolite framework. The La $3d_{5/2}$ BE would indicate that lanthanum is at exchange position into the mordenite in the fresh solid. The increase of the BE after reaction indicates a different chemical environment that could be the result of some interaction with indium species. This fact together with the concentration increase of $(InO)^+$ species with low BE would confirm the electronic interaction of both elements.

Table 3
XPS data.[a]

Sample	Binding energy (eV) Atomic (%)			Si/Al[d]	In/Si[d]	La/Si[d]	La/In[d]	In/Al[d]
	In $3d_{5/2}$[b]	In $3d_{5/2}$[c]	La $3d_{5/2}$					
InHM-f	–	446.4 100%	–	10.5	0.0019	–	–	0.020
InHM-u	444.2 4%	445.9 96%	–	6.7	0.0041			0.027
LaInHM-f	445.3 23%	446.2 77%	836.8 0.38%	9.7	0.0035	0.019	5.43	0.034
LaInHM-u	445.2 65%	446.3 35%	837.2 0.20%	10.5	0.0023	0.008	3.48	0.024

[a] For all samples, the binding energies of Al, Si, O and C were the following: C 1s = 284.8 eV, Al 2p = 74.1 ± eV, Si 2p = 102.6 ± 0.1 eV, O 1s = 531.9 ± 0.1 eV.
[b] Low binding energy (In_2O_3 or In^+ species).
[c] High binding energy ($(InO)^+$ or In_xO_y species).
[d] XPS surface atomic ratio.

After reaction, the Si/Al ratio of the InHM catalyst decreased, suggesting that the surface aluminum probably increased due to a dealumination process. Consequently, in the InHM-u solid some Al species deposition on the external surface could occur. The dealumination of the support was found to be one of the key processes occurring during deactivation of Cu-zeolite catalysts used for SCR [47]. The partial dealumination could cause the migration of indium ions into a more associate state under SCR conditions [48]. After the reaction 4% of exchanged $(InO)^+$ appear as In_2O_3 and the In/Si ratio increases. These two results, decrease of surface Si/Al and increase of In/Si ratio, could support the dealumination process and the migration of indium from the exchanged position as will be later confirmed by some extent agglomeration observed by TEM. With the incorporation of lanthanum by ionic exchange on the InHM catalyst the Si/Al ratio did not change significantly after reaction ruling out dealumination processes.

3.3. BET area and pore volume

No significant difference on the BET area was found between the fresh and used InHM catalysts prepared by ionic exchange, neither on the pore volume values (Table 4). The dealumination processes that suffer this catalyst during reaction sustained by XPS and FTIR (shown later) would not destroy the matrix structure and would produce small Al extra-framework particles that do not occlude the pores. But in the used LaInHM, the BET area and the pore volume decreased (20% and 18% respectively). The loss of the BET area and the pore volume of the zeolitic catalysts, generally are the result of the presence of strong dealumination process. So it could be suspect that this process slightly occurred in the LaInHM catalyst. During the La exchange different hydrated lanthanum species are present into the synthesis suspension of the catalysts. The smallest hydrated specie is the hexaquo ion, $La(H_2O)_6^{3+}$, with d ≈ 6.6 Å and it is probably the main ion exchanged species that is able to get into the main channel of the zeolite (6.7 × 7.0 Å). There is less probability that La occupies smaller cavities (5.7 × 2.6 Å and 3.7 × 4.8 Å) [49]. The decrease of the BET area and pore volume can be also related to the formation of particles with higher sizes in the main channels under reaction stream than the ones present in the fresh catalysts.

3.4. XRD results

The XRD patterns were recorded over a range of 2θ angles from 5° to 40° and crystalline phases were identified using the JCPDS file 43-0171 corresponding to mordenite. In addition, the cell parameters were calculated from (200), (020) and (202) peaks using the software provide by Shimatzu XRD spectrometer. The crystallinity of the modified mordenite was calculated by comparing the sum of the peak areas of (150), (202), (350) and (402) (22–32° 2θ) with respect to calcined H-Mordenite.

Fig. 1 enables to follow the ex-situ structural changes of HM induced by In and/or La and by the rigorous reaction conditions. X-ray diffraction patterns of LaIn-containing samples (Fig. 1) showed

Table 4
Volumetric results and data obtained from XRD patterns.

Catalysts	N_2 adsorption		XRD		
	Area BET (m^2/g)	Pore volume (cc/g)	Crystallinity (%)	FWHM [202] -[111] line	Unit cell volume ($Å^3$)
HM	521	0.247	100	0.262–0.379	3126
LaHM-f	n.a	n.a	93	0.231–0.305	3089
InHM-f	525	0.244	97	0.215–0.303	3082
InHM-u	499 (↓5%)	0.244	86	0.227–0.343	3099
LaInHM-f	506	0.262	93	0.184–0.257	3091
LaInHM-u	404 (↓20%)	0.215 (↓18%)	86	0.244–0.299	3098

in all cases only peaks corresponding to the zeolite matrix. Peaks ascribed to lanthanum and indium oxide or other La or In-based phases were not observed in the XRD patterns of fresh and used catalysts. Nevertheless, the presence of La or In phases of low crystallinity or crystalline phases with small crystallite size could not be excluded.

The XRD pattern of HM was included for comparison purposes. It is clearly seen that the exchange of indium and lanthanum conduces to the decrease of the intensities of characteristic zeolite peaks. The loss of intensity is higher after the successive exchanges and also after reaction. This fact might be also due to the cation exchange or some dealumination process [50,51].

The baseline of the XRD patterns of the used catalyst showed a low increment. There are two causes that may conduce to this feature: (i) some breakdown after the different treatments (exchange, calcination, reaction) and (ii) the dealumination of the mordenite framework.

In order to evaluate the crystallinity of the used and fresh samples, the cell parameters and the cell volume were calculated from the XRD data (Table 4). The catalytic cell volumes slightly increased after reaction, but this result does not conduce to speculate with the presence of a drastic dealumination process since the crystallinity did not decrease significantly after reaction.

Therefore, according with these results it can be concluded that the applied wet reaction condition drives a mild structure change on the zeolitic matrix (Fig. 1, Table 4).

3.5. Pyridine desorption. Py-TPD

The adsorption energies of pyridine on Brönsted (Br) and Lewis (Lw) acid sites are very similar and high temperatures (750–820 °C) are needed to desorb all the adsorbed pyridine [52]. So each TPD peak resulting from the deconvolution does not correspond to a single type of site, but is rather the result of the distribution of sites that have comparable adsorption energies (Fig. 2).

Pyridine desorption results are reported in Table 5. After the In exchange into the mordenite matrix, the total amount of acid sites increased respect to the starting support (μmol Py/g cat). But the

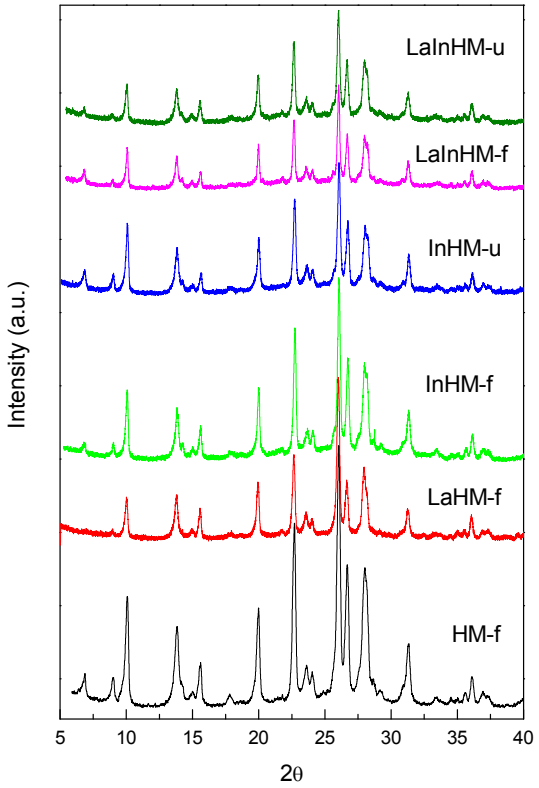

Fig. 1. XRD patterns of the fresh and used prepared solids.

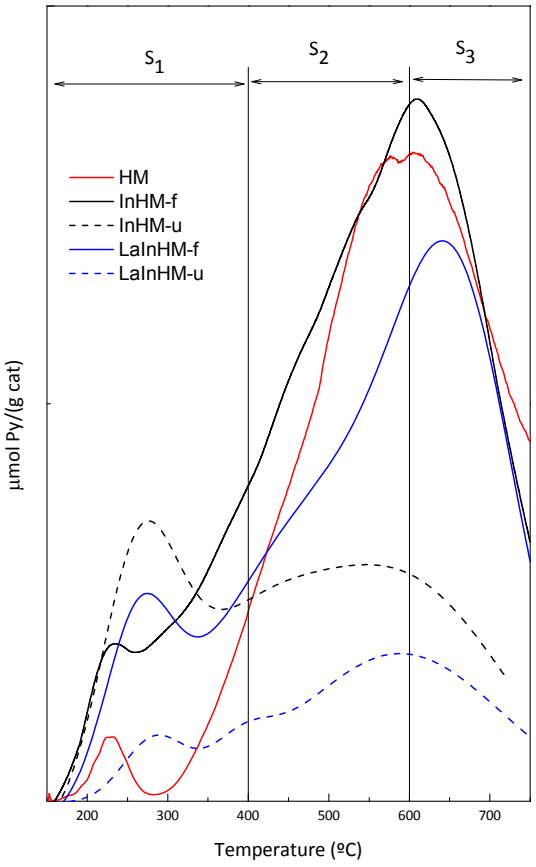

Fig. 2. Pyridine desorption profiles of the support and the fresh and used catalysts.

Table 5
Relative quantity of acid sites present in the studied catalysts.

Catalyst	μmol Py/μmol total Py (%)[a]			μmol Py/g cat
	S_1 100-400 °C	S_2 400–600 °C	S_3 600–750 °C	
HM	1.94 (230 °C)	19.2 (445 °C sh)	79 (610 °C)	0.75
InHM-f	18.6 (230 °C)	13.5 (460 °C)	68 (600 °C)	0.98
InHM-u	40.6 (276 °C)	59.3 (550 °C)	–	0.55
LaInHM-f	7.28 (276 °C)	63.6 (460 °C)	29 (645 °C)	0.84
LaInHM-u	15.6 (290 °C)	84.4 (585 °C)	–	0.26

[a] In brackets the maximum temperature in each S_i range.

presence of La after In exchange led to a total acidity decrease, compared with the InHM. After reaction, the acidity in the LaInHM catalyst drastically decreased (70%) while in the used InHM solid this value dropped to almost 44%. In order to further investigate the acidity modifications of the catalysts after reaction, the Py-TPD profiles were divided in three zones taking into account the desorption temperature ranges: S_1 sites, with 100–400 °C Py desorption, which could be considered weak acid sites; S_2 sites, with 400–600 °C Py-TPD, which could be considered moderate acid sites and S_3 sites, with 600–750 °C Py desorption, which could be associated to strong acid sites [52]. No evidence of the pyridine decomposition at high temperature was observed.

After the cation incorporations into the mordenite and after reaction, not only did the Py consumption modify but also the distribution of the different kind of acid sites. In fact, after indium and lanthanum exchange the strong acid sites dropped 14% after indium incorporation and 63% after the exchange of La into InHM. After reaction the strongest acid sites disappear in both catalysts (InHM-u and LaInHM-u), this effect may be due the result of the dropping of the specific surface area (because of dealumination observed in InHM-u) or due to the agglomeration of particles on the mordenite surface which make the Py adsorption (TEM results) difficult. It could be suggested that the partial blockage due to dealumination process conduces to a decrease of the surface area and to a loss of pyridine adsorption capacity. On the other hand, with the dealumination, weaker acid sites are developed (EFAl), and, as a consequence of both processes, a decrease in the total amount of acid sites is observed. Moreover, the environmental changes into the matrix (observed by XPS) also take part in the acid sites distribution.

Hartford et al. [53] studied the La incorporation into ZSM-5 and deduced that the lanthanum exchange reduces the number of both Lewis and Brönsted acid sites on the catalyst, suggesting that the La ions function as weak acid sites.

The assignment of the distribution of Sn (S1, S2 and S3) of acidic sites to specific type of centre (i.e. Br or Lw) is hardly attainable on the basis of TPD results only. Observations by FTIR are needed for a good discrimination between sites of different natures. However the results obtained with TPD of pyridine can provide some evidence of quantitative acid cites present in each catalyst (fresh and used).

4. FTIR results

4.1. Unperturbed samples (before CO adsorption)

The spectra in the 3000–3600 cm^{-1} interval of the starting mordenite (HM) is attributed to either SiOH groups in the framework defect sites (nests) interacting through hydrogen bonds or to distorted bridged hydroxyl acid groups interacting with oxygen atoms of the framework. Particularly the wide band at 3300 cm^{-1} may be associated with Brönsted acid groups in defective sites (nests included). The frequency of these groups shifted downwards with respect to “normal” species because of weak hydrogen bond interaction with other groups.

The very strong band at 3605–3610 cm^{-1}, is due to the bridging Si–OH–Al groups that are exclusively on the inner surface and possess a strong Br acidity. Such band is characterized by a tail towards lower frequencies due to the bridging OHs (3530–3570 cm^{-1}) located in the so-called side pockets [53].

The OH vibration of free silanols SiOH (silanols not interacting through hydrogen bonds, because they are isolates or in terminal positions) appears as a wide band at 3720–3740 cm^{-1} interval [54].

The water adsorption conduces to some typical bands at 3710, 2700 and 1600–1800 cm^{-1} range. The bands at 2700 and 1600–1800 cm^{-1} (not shown) have not been observed in any of the samples analyzed by FTIR, so it can be assured that the vacuum wafer pre-treatment at 400 °C lead to the total elimination of the adsorbed water.

After the thermal pre-treatment of wafers in high vacuum, an adsorption band at 3660–3680 cm^{-1} due to the presence of hydroxyl groups in extra lattice aluminum (EFAl) was observed. This band also occurs when zeolites are treated under rigorous reaction conditions (high temperature and high water concentration in the reaction stream), typical of dealumination process. Hence, on the HM sample the presence of a small contribution of the band located at 3660–3680 cm^{-1} may be due to the treatment followed before the FTIR observations.

Particularly in the OH stretching region of our evacuated HM wafer at 400 °C (Fig. 3A) the FTIR spectra consisted of bands at 3740, 3660 and 3610 cm^{-1}. The band at 3740 cm^{-1}, asymmetric in the low-frequency side, corresponds to the O–H stretching modes of terminal OH groups (silanols) located on the external surface of the matrix; while the band at 3610 cm^{-1} is assigned to O–H stretching of bridged hydroxyls Si(OH)Al, characteristic of Br acid sites located in the main channels. This band presents a tail to lower frequencies (~3580 cm^{-1}) corresponding to Br sites at smaller channels (side pockets) [55]. It was also reported for other zeolites that the broad band in the 3000–3500 cm^{-1} interval corresponds to either SiOH groups in framework defect sites (nests) interacting through hydrogen bonds [56] or to distorted bridged hydroxyl acid groups interacting with oxygen atoms of the framework [57]. The broad adsorption peak at 3660 cm^{-1} would indicate the presence of extra-framework Al^{3+} [58,8]. Some authors named the 3578 and 3610 cm^{-1} bands as low (LF) and high (HF) frequency bands, where LF(OH) has lower acidity than HF(OH) [59,60].

The contribution of the 3610 cm^{-1} band decreased after the exchange of indium into HM (40%–30%) because of the indium exchange process (Table 6 and Fig. 3A and B). Although by Py-TPD, a total increase in the acid concentration due to the incorporation of indium was observed. These results are not contradictory because the acid sites evaluated by FTIR at 3610 cm^{-1} correspond only to Br sites, while the Py-TPD gives the total amount of acid sites (Br and Lw).

The InHM-u catalyst showed an increment of the 3660 cm^{-1} band in the OH species adsorption range (Fig. 3B). The total area of the OH range decreased three times and the ratio between the 3610 cm^{-1} contribution and the 3660 cm^{-1} decreased from 5.3 to 2.4 in comparison with the fresh solid in which there was no evidence of EFAl (extra-framework Al) entities. On the other hand, the LF acid sites (c.a. 3550 cm^{-1}) also dropped after reaction. As a result, it could be concluded that after reaction in the InHM catalyst not only did the acidity decrease in agreement with the Py desorption results but also a dealumination process could have occurred.

The LaInHM used and fresh catalysts showed a very broad area in the FTIR region of OH species. In both solids a band at 3520–3550 cm^{-1} is observed which correspond to lanthanum at exchange positions (Fig. 3C). In fact, Moreira et al. [41] related this

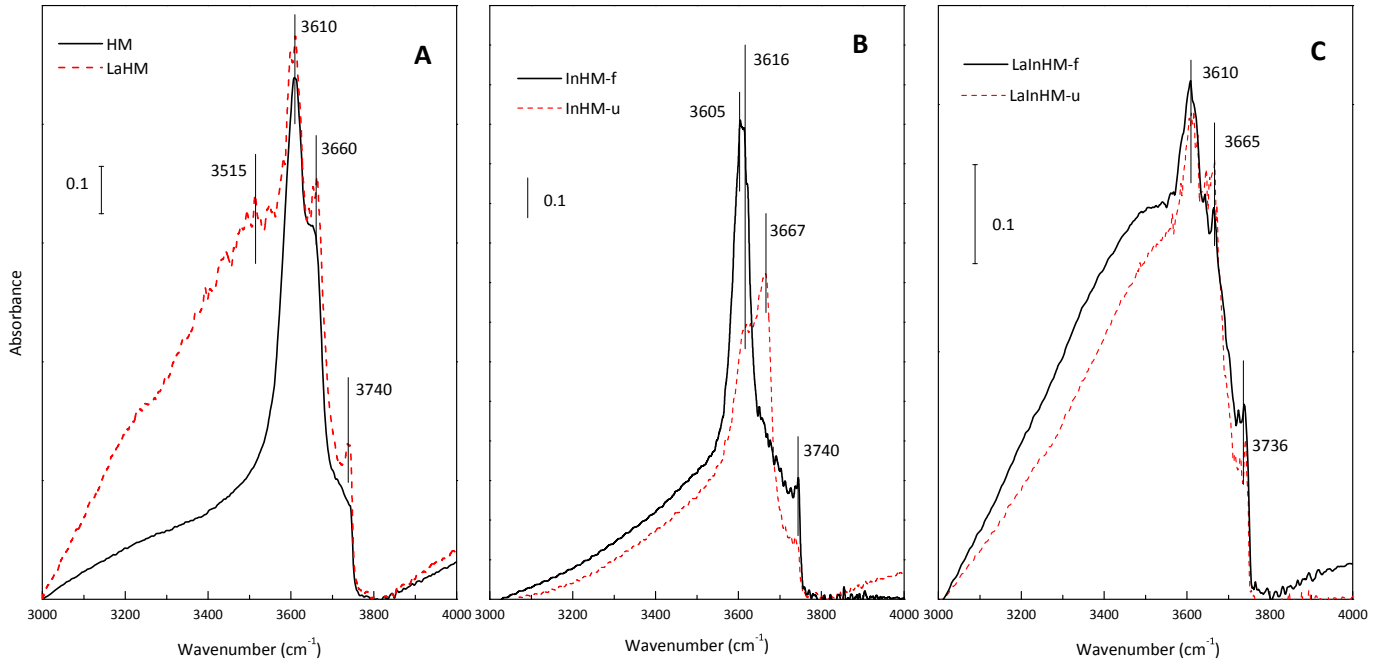

Fig. 3. FTIR spectra of the fresh and used catalysts. A: HM and LaHM, B: InHM-f and InHM-u, C: LaInHM-f and LaInHM-u. Before FTIR observation all solids were evacuated under high vacuum at 400 °C overnight.

band to La species, and they speculated on the presence of oligomerized La species on large Y-zeolites cages.

It has been reported that the lanthanum ion exchange increases the number of weak acid sites and decreases the number of strong acid sites. Due to the large size of aqueous lanthanum species, $La(H_2O)_6^{3+}$ (d = 6.6 Å) the La ion-exchange is supposed to occur on the outer surface of the zeolite [61]. This result is in agreement with the Py-TPD results, in which the S2 sites increase after the lanthanum ion-exchange.

In order to confirm this speculation, the LaHM sample was also analyzed by FTIR spectroscopy (Fig. 3A). In the calcined LaHM solid similar broad band at LF was also observed. The area of the peak corresponding to the maxima at c.a. 3520 cm^{-1} in all La containing samples was higher than the corresponding to strong Br acid sites (3610 cm^{-1}). This confirms the lower acidity of the LaInHM samples calculated by Py-TPD. It is important to take into account that the inhomogeneity of OH species distribution into the mordenite matrix difficults the identification of the acidity strength [54].

The ion exchange on the mordenite and the reaction under rigorous conditions, conduce to a new distribution between the LF and HF acid sites. On the other hand, the dealumination process resulted higher in the InHM than in the LaInHM catalyst. In fact the proportion of EFAl species increased from 5.5 to 13.9% in the InHM catalyst after reaction (Table 6). These results are in agreement with XPS observations.

Table 6
Related areas of the OH range spectra (3000–4000 cm^{-1}).

Catalyst	A_{3540}/A_T (%)	A_{3610}/A_T (%)	A_{3660}/A_T (%)
HM-f	0	39.7	8.1
LaHM-f	49	35.5	n.d
InHM-f	27.7	29.3	5.5
InHM-u	20.2	33	13.9
LaInHM-f	31.9	13.2	8.6
LaInHM-u	34.1	12.4	9.1

In order to gain further insight on the effect of lanthanum on the modifications of the InHM structure, CO adsorption monitored by FTIR experiments were performed. CO is a very good probe molecule for the elucidation of the type of acid sites present into the matrix (Lw or Br).

5. CO-FTIR adsorption

CO adsorption results in the formation of CO–OH complex which lead to two regions in the CO–OH spectrum: (i) CO perturbation of –OH groups with typical bands at 3660 to 3300 cm^{-1} range which position depends on the acidity strength and (ii) the characteristic of the stretching of CO bands located between 2100 and 2240 cm^{-1}. The position of the latter bands depends not only on the strength of the acid sites but also on the nature of the exchanged species into the matrix. The broadness of the O–H stretching band at 3610–3616 cm^{-1} and its asymmetry on the low frequency side conduce to a band at ca. 3340 cm^{-1} resulting from the CO–OH interaction. Both the broadness and asymmetry of the IR absorption band corresponding to bridged hydroxyl groups provide clear evidence for the heterogeneity of the Br sites [62,63].

The CO adsorption bands (2240-2100 cm^{-1}) of the fresh and used catalysts are shown in Figs. 4–6, while the spectra of the OH sites altered by the CO adsorption are shown in Fig. 7.

In order to have a reference, the CO adsorption on calcined HM and LaHM solids were carried out.

HM. Figs. 4A and 7.

The presence of CO yielded several bands (Fig. 4A), whose intensities increased when the CO pressure increased. The bands at 2222 and 2195 cm^{-1} appeared when 5 Torr of CO was added, while the signals at 2168 and 2139 cm^{-1} emerged after higher CO pressure. The former might result from two components, where the low frequency band at 2168 cm^{-1} is assigned to CO adsorbed on Br acid sites located into the side pockets, and the band at high frequency (2170 cm^{-1}) was the adsorption signal of CO–OH on the main channel. Then the signal at 2139 cm^{-1} is attributed to CO as a

pseudo-liquid state. The bands at 2222 and 2195 cm^{-1} were associated to CO on Lewis acid sites and their intensities almost did not change when the CO pressure increased.

The ν_{CO} at 2168 and 2158 cm^{-1} were related with the sites at ν_{OH} at 3610 and 3578 cm^{-1} respectively. Bordiga et al. [64] also observed on NaMordenite two bands at 2178 and 2163 cm^{-1} assigned to the CO adsorption on Na^+ in the main channels and into the side pockets respectively. In the HM sample of this work, these bands were not observed, suggesting that the NH_4^+ exchange in the parent NaMor resulted effective.

The OH groups vibrating in small pores (and cages) underwent a red shift compared to the frequency at which their vibration would occur in larger cavities. In fact the 3610 cm^{-1} band (Fig. 3A) was asymmetric on the low-frequency side and can be resolved into two components centered at 3610 and 3578 cm^{-1}, respectively (not shown). The observed broadness of these bands suggests a small heterogeneity of both sets of OH groups. The addition of CO (Fig. 7) conduces to a decrease of the 3610 and 3578 cm^{-1} bands, and to the formation of a broad band growing at c.a. 3350 cm^{-1} which is the sum of the contribution of two bands (c.a. 3437 and 3317 cm^{-1}, not indicated). This suggests the formation of new hydrogen-bonded CO–OH species. The large width of this new band evidences the inhomogeneity of OH type groups. The subtraction of unperturbed wafer to the CO adsorbed spectra also showed that CO interacts with silanol species defined by the band at 3660 cm^{-1}.

LaHM. Fig. 4B.

The adsorption of CO at RT on fresh LaHM (Fig. 4B) shows a strong band at 2189 cm^{-1} associated with La at exchange. At higher CO pressure a shoulder appears at 2166 cm^{-1}, suggesting that there is a less accessible La adsorption site in the matrix. A weak CO-EFAl signal also appears at 2220 cm^{-1}. The frequency of this band does not change with the CO pressure (from 5 to 100 Tor), indicating that CO adsorbed on isolated La sites.

InHM-f. Figs. 5A, 7A and 7C.

The analysis of the ν_{CO} region (Fig. 5A) on this sample conduces to spectra similar to the calcined support (HM) but the signal of CO adsorbed on the OH in the small channels appears as an evident shoulder at 2156 cm^{-1}.

The CO adsorption bands at 3740 and 3608 cm^{-1} in the InHM-f were negative after the subtraction of the unperturbed spectrum; this is due to the CO adsorbed on the sites corresponding to 3720 and 3610 cm^{-1} of the unperturbed wafer. However, the CO adsorption led to positive band at 3494 and 3365 cm^{-1} which correspond to the CO stretching interacting with OH species located at the side pockets and into the main channels respectively. It can be observed that the peaks are broad, meaning a high heterogeneity of the distribution of the species (Fig. 7A and C).

InHM-u. Figs. 5B, 7A and 7C.

After reaction the characteristic band of CO adsorption on Br acid sites centered in 2168 cm^{-1}, split into two well defined bands at 2176 an 2159 cm^{-1} (Fig. 5B). This suggests that there were some changes in the surroundings of the OH located into the main channels and into the side pockets. It could be suspected that after reaction the indium species migrate to outer positions and conduce to CO molecules polarized by $(InO)^+$ cations located in the main channel and therefore $(InO)^+$ behave as Lewis acid sites [65]. Although it should be noted that the signal at 2173 cm^{-1} did not appear in the fresh sample, this might be from the formation of In species with a structure similar to the In bulk oxide, as it was observed by XPS. This evidence may be supported by the results reported by Areán et al. who observed similar behavior on Ga/HZSM catalysts [63].

The adsorption of CO on the OH(3730), OH(3666) and OH(3636) sites observed on the unperturbed solid spectrum (Fig. 3), conduced to three well defined negative bands for all CO pressure. From 3578 cm^{-1} frequency the adsorption bands became positive, and also the CO–OH interaction peaks at 3440 cm^{-1} and 3282 cm^{-1} which correspond to OH(3553) and OH(3636) sites respectively. It should be noted that the Brönsted site frequency shifted to a higher

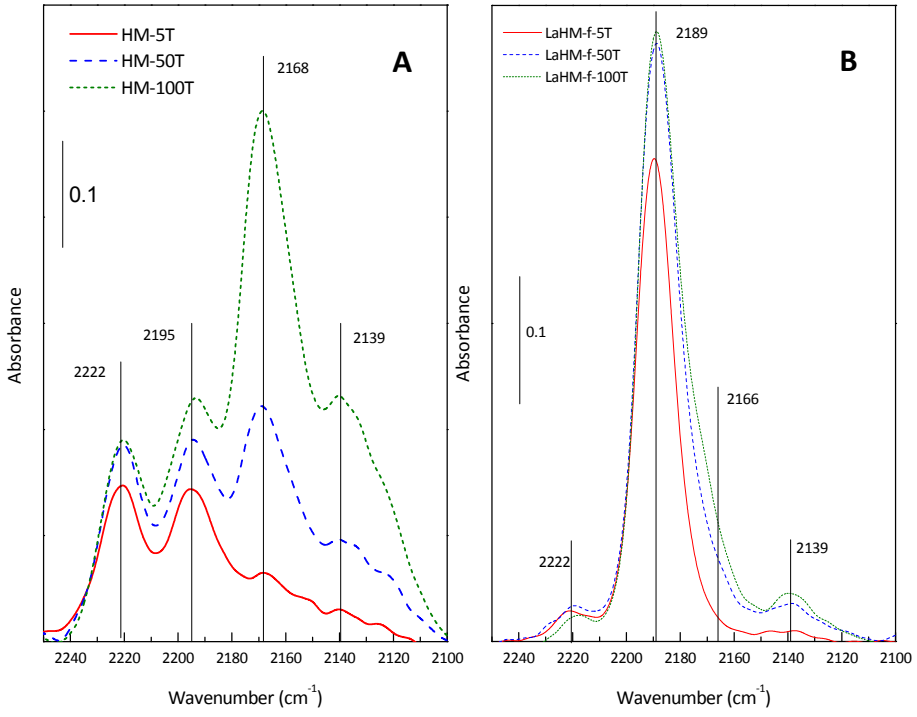

Fig. 4. FTIR spectra of CO adsorption of the reference samples. A: Support HM, B: LaHM.

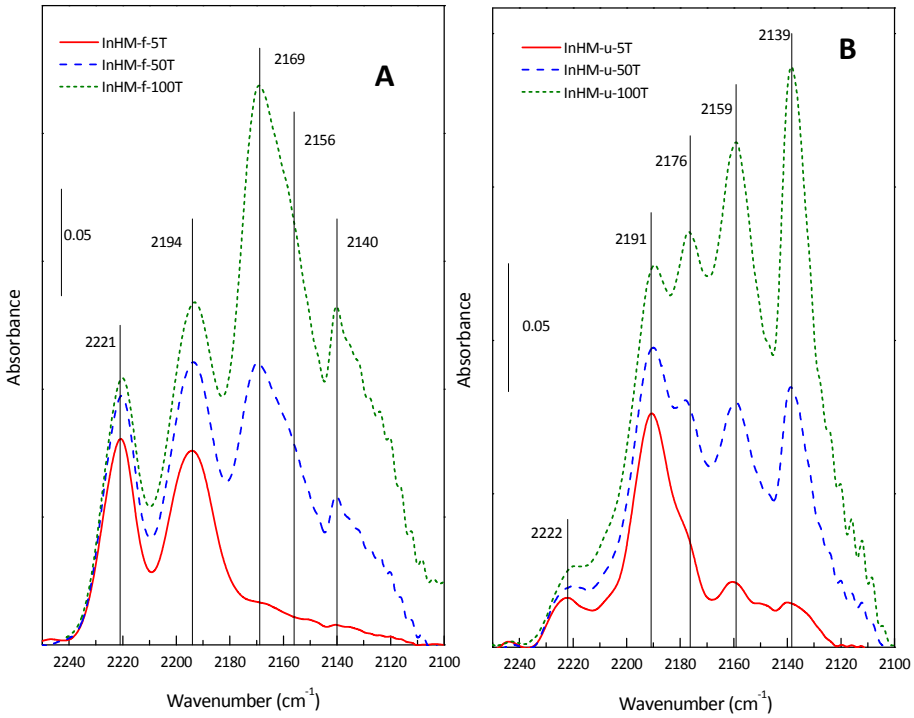

Fig. 5. FTIR spectra of CO adsorption on InHM catalysts. A: Fresh, B: Used.

value: from 3608 to 3636 cm^{-1}. This could suggest that after reaction there was some modification around the environment of such acid sites (Fig. 7A and C).

The adsorption intensity is lower than the fresh InHM, which is in agreement with the BET and XPS results; in which the decrease of surface area and the oxide type indium species were observed on the solid surface.

LaInHM-f. Figs. 6A, 7B and 7D.

The spectra taken in the ν_{CO} adsorption range (Fig. 6A) were also notably different from those obtained on the HM and the InHM fresh and used catalysts. In fact there is a main adsorption band centered at ca. 2186 cm^{-1}. This band was broadened towards lower frequencies while the CO pressure increased. The contribution of the tail of such band could be fitted into two bands after the

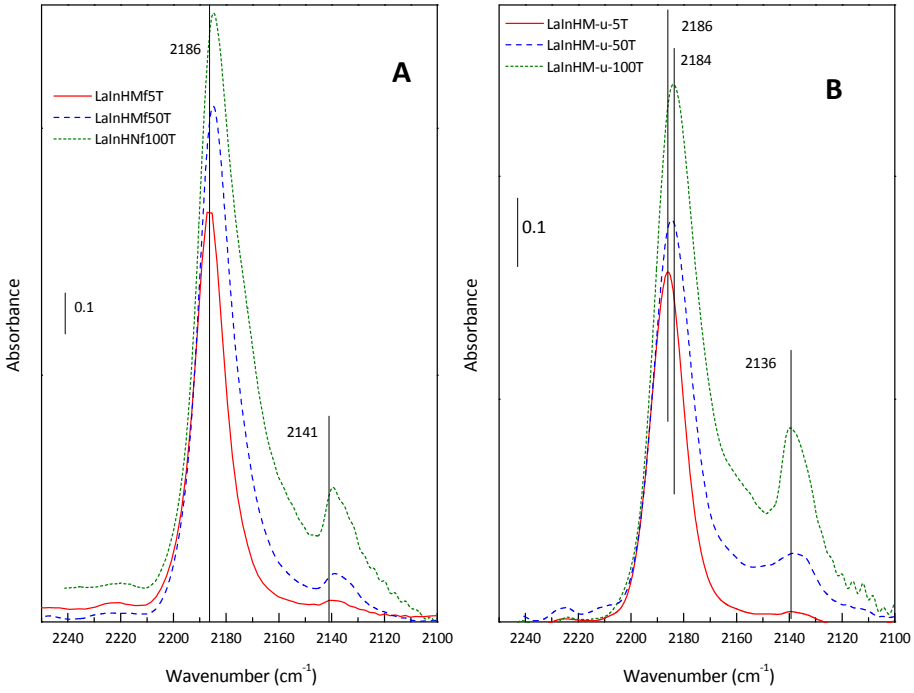

Fig. 6. FTIR spectra of CO adsorption on LaInHM catalysts. A: Fresh, B: Used.

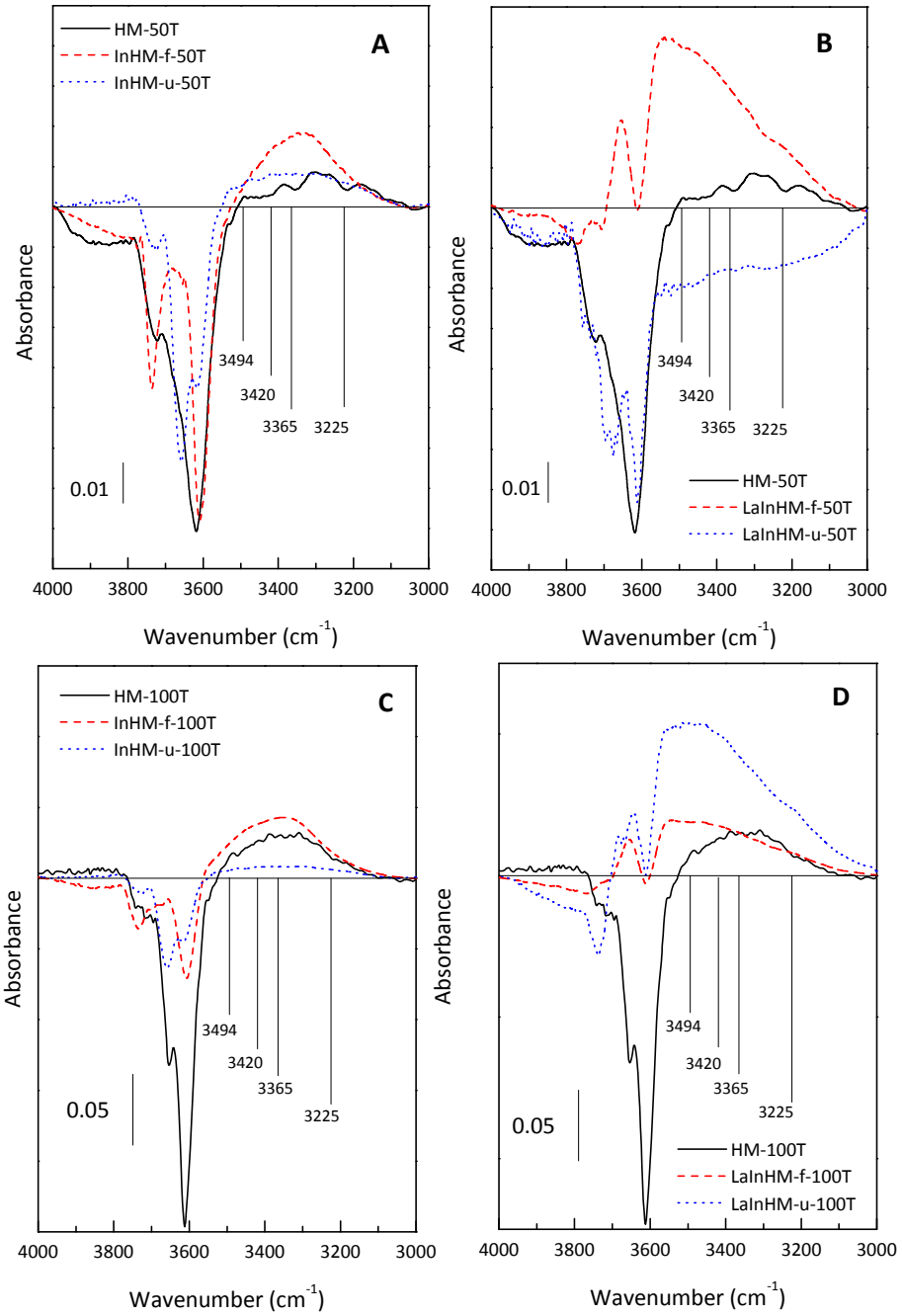

Fig. 7. OH region FTIR spectra that resulted from the subtraction of the adsorbed wafer with CO (50 and 100 Torr) and the unperturbed sample. A: InHM-f-50T, B: LaInHM-f-50T, C: InHM-f-100T, D: LaInHM-f-100T. The spectrum corresponding to the support HM was included for comparison purposes.

addition of 50 Torr of CO: 2185 and 2165 cm^{-1}. The former attributed to lanthanum at exchange position with Lewis acid site conduct [64] and the latter to CO interacting with bridging OH groups coming from NH_4^+ cations not exchanged with lanthanum and indium located into the main channels. CO adsorption band for the CO–OH into the side pockets was not detected, probably because the lanthanum or oxide type indium (see XPS results) species blocked these small channels.

The ratio between the main band and the located at 2220 cm^{-1} resulted notably higher than the observed in the HM and InHM solids.

The presence of 5 Torr of CO affected the OH(3735), OH(3670), OH(3610) and OH(3545) sites, as evidenced by the negative area after subtraction of the spectrum of the clean wafer at the full range. The positive broad peak may be fitted into two peaks at 3419 and 3232 cm^{-1} which suggests the modification of the O–H bond from the OH sites with different acid strength interaction with the presence of the CO (Fig. 7B and D).

The spectra resulted from the subtraction are different from the obtained with the LaHM-f. Therefore, it could be suspected that there is some interaction between In and La into the mordenite channels.

Some effect of La on the InHM was evident when comparing the intensity of the spectra of LaHM with that of LaInHM. In fact the adsorption intensity in the latter spectra is higher than in the former. On the other hand, in the $\nu_{CO\text{-}OH}$ range the adsorption

Table 7
Acidic strength of the Br sites into the mordenite main channels and side pockets.

Catalyst	$\Delta\nu_{CO\text{-}OH}$	
	Main channel	Side pockets
HM	304 (302)	144 (92)
LaHM-f	350	
InHM-f	264 (251)	107 (102)
InHM-u	301 (290)	88 (73)
LaInHM-f	280 (235)	44
LaInHM-u	288	57

intensity on LaHM-f was very low and the CO interaction with OH hardly was evidenced after exposure to 100 Torr of CO (not shown).

LaInHM-u. Figs. 6B, 7B and 7D.

The CO adsorption frequencies resulted similarly although with lower intensity than in the fresh LaInHM. The CO adsorption at the OH region presented notable differences between the mono and bimetallic samples. At low CO coverages, the interaction of CO with Lw sites dominates over the Br sites [66] (Fig. 6B).

The bands at 3730, 3664 and 3610 cm^{-1} resulted negative for all CO pressures, while only at 100 Torr positive bands arise at 3479 and 3339 cm^{-1} due to the CO contribution on 3534 and 3618 cm^{-1} OH-sites. This effect of the negative areas could be due to the decrease of the catalyst specific area and/or pore volume after reaction. High pressure is needed to distinguish CO interaction with OH because of the low CO accessibility to the acid sites (Fig. 7B and D).

5.1. Comparison of acid site strength

The preceding results suggest that the presence of lanthanum and/or indium into the fresh and used catalysts conduce to significant modifications on acid sites into the mordenite. These changes may be the result of the presence of indium and/or lanthanum at exchange sites interacting with nearby OH acid sites or to structural modifications leading to changes of the acidic strength. Nevertheless, it should be taken into account the structural modifications from the process of dealumination or cations mobility produced by the hydrothermal treatment during the reaction.

The types of hydroxyl groups occurring into the mordenite are (i) SiOH from defect, outer surface or silica impurities, (ii) AlOH from no-skeletal alumina and silica alumina impurities (extra-framework Al, EFAl) and (iii) SiOHAl from the mordenite skeleton. As well, it is widely known that the acid strength is in the order: SiOHAl > AlOH > SiOH [67,68].

On the other hand, the γ_{OH} shift due to the perturbation with CO reflects the acid strength of the hydroxyl groups. It is established that the lower the red shift ($\Delta\gamma_{CO\text{-}OH}$), the lower the site acidity. The frequency assignments to each OH species γ_{OH} are shown in Table 7, together with $\nu_{CO\text{-}OH}$ bands driven from the formation of CO–H-bonded complex. The γ_{CO} originated by the CO adsorption is also reported.

In this vein, we could speculate with the characteristic of the acid sites present in each studied sample in this work. From the fitting of the 4000–3000 cm^{-1} interval of the spectra obtained after the subtraction of unperturbed samples to the spectra after the CO adsorption, we can report two main broad peaks that are present at all CO pressure: (i) 3365–3225 cm^{-1} and (ii) 3420–3494 cm^{-1}, both ranges were assigned to OH into the main channels and into the side pockets respectively. Then, in the 2050–2100 cm^{-1} range the CO vibration were: 2170 and 2158 cm^{-1}, whereas for catalysts containing lanthanum the main band is at 2184 cm^{-1}.

The band at ca. 2156 was related to the 3660 cm^{-1} assigned to EFAl sites. In all samples the bands at 2180–2150 cm^{-1} range were broad, which could indicate that there was a contribution of EFAl entities together with other acid sites. However, the spectra obtained with the CO adsorption on InHM-u revealed a clear presence of EFAl groups as it was also observed in Fig. 3B (InHM-u spectra) and in agreement with XPS results.

Table 7 shows the $\Delta\gamma_{CO\text{-}OH}$ and the following experimental evidence can be distinguished: (i) I all samples the OH bands corresponding to OH at both positions, in the side pockets and in the main channels presented the O–H bond alteration because of the CO presence, and (ii) In all samples, the strength acidity calculated by fitting the resulted spectra of the adsorption of 100 Torr followed the same trend of the integration results obtained from the spectra with 50 Torr of CO (number in brackets).

It should be noted that for all samples the acidity from the hydroxyl species placed in the small cavities is lower than the observed in the big channels. The highest strength was observed in the calcined unmodified support (HM). The incorporation of indium conduced to a decrease of the acidity (InHM-f), but after the lanthanum exchange the strength of Brönsted acid sites was partially recovered (Table 7). After reaction the InHM-u and LaInHM-u samples increased the acidity into the main channels. It should be also remarked that the OH species into side the pockets lose their acidic capacity compared to the starting mordenite, being more drastic in the lanthanum-containing catalysts.

The presence of lanthanum on the InHM catalyst not only reduced the number of strong acid sites (Brönsted) but also the total acidity (Table 6). On the contrary, the exchange of La alone into the HM increases notably the acidic strength. The lanthanum exchanged process might be produced on the surface of the mordenite because of the size of the ionic species of the exchange solution.

The acid strength associated with the OH into the main channels can be ranked as follows:

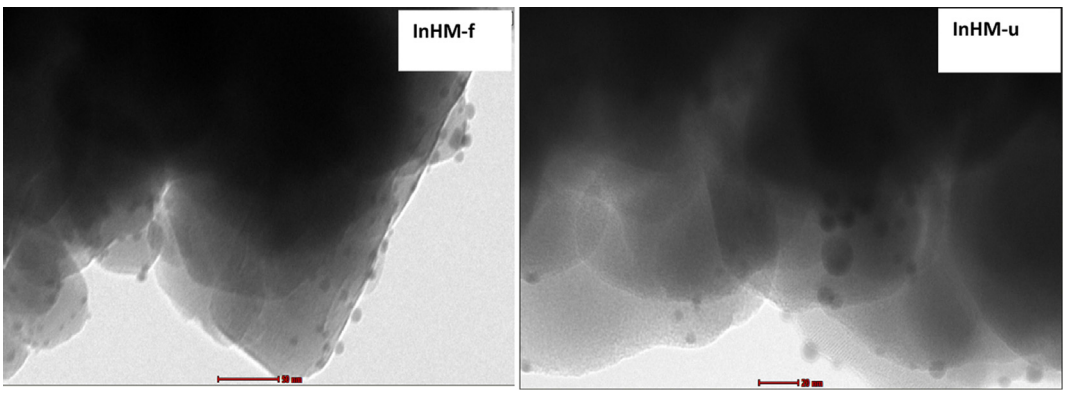

Fig. 8. Transmission Electron Microscopy (TEM) images. The bar in the left picture correspond to 50 nm and in the right to 20 nm.

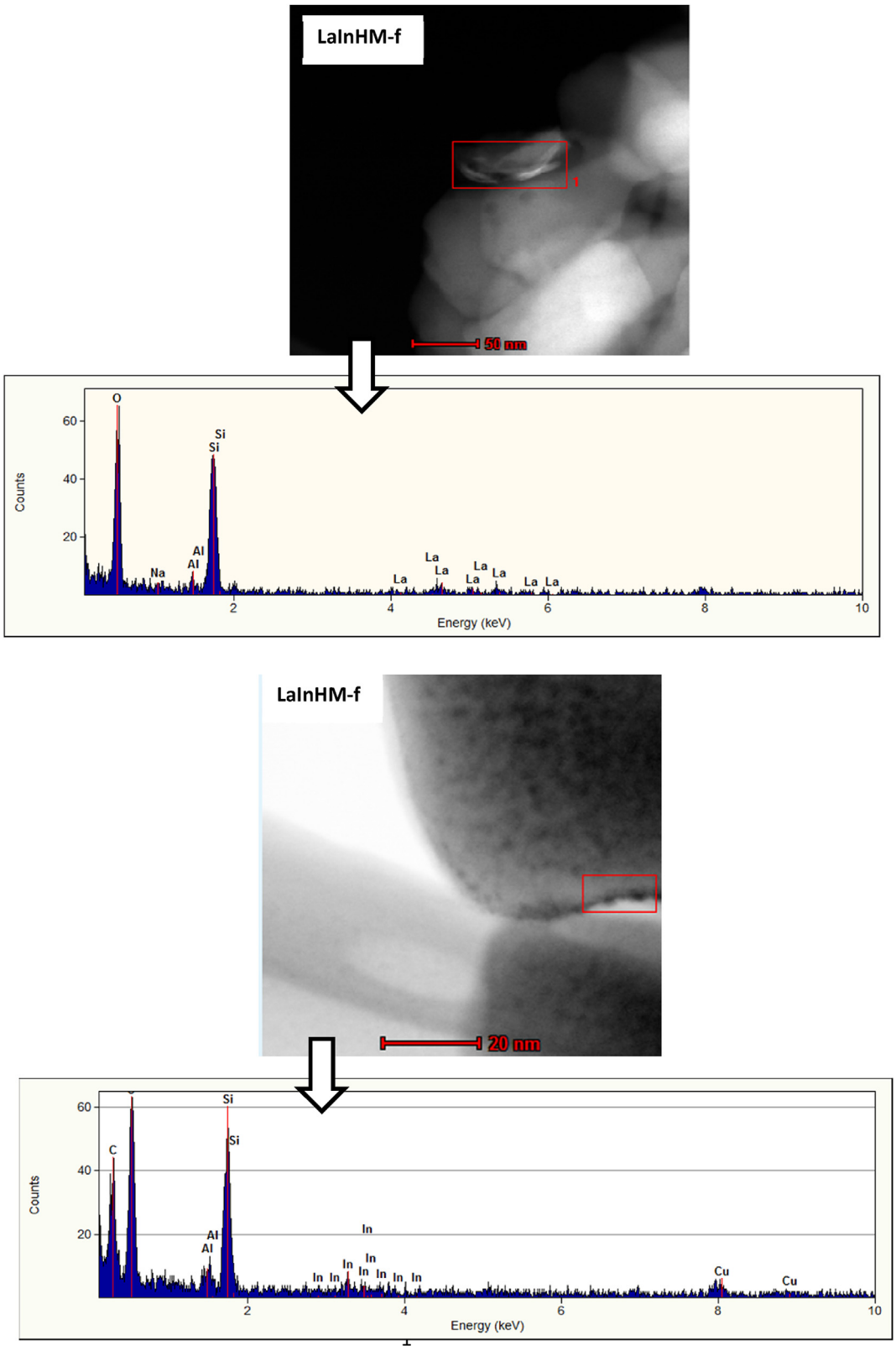

Fig. 9. Transmission Electron Microscopy (HRTEM) images and EDX spectra of LaInHM-f and LaInHM-u catalysts.

LaHM-f > HM > InHM-u > LaInH-u > LaInH-f > InH-f. As a result, the La–In interaction affects the acidity as also the wet reaction condition.

Consequently, the interaction of protons from mordenite (HM) and La ions from LaHM-f together with the In ions from InHM-f conduced to a catalyst (LaInHM-f) with an acid strength intermediate between the starting monometallic solids.

All of these considerations do not exclude the broadness of the OH vibration bands which is due to interaction of these sites with

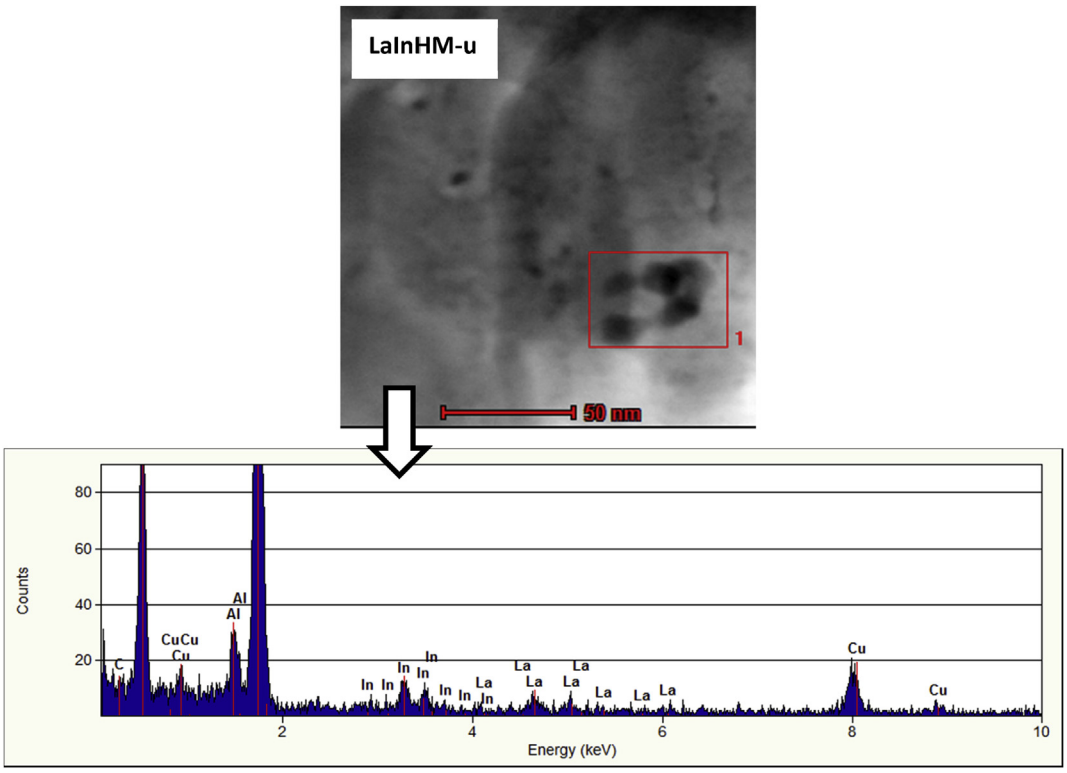

Fig. 9. (*continued*).

the complex neighborhoods into the zeolite framework, but we believe the foregoing arguments are worth considering and are full supported by well-known references.

5.2. Transmission Electron Microscopy (TEM) images

In order to support the foregoing hypothesis the transmission Electronic Microscopy technic was also applied.

The InHM-f microscopy shows scarce number of particles distributed on the catalysts with sizes from 4 to 7.5 nm (Fig. 8). In the used catalyst the concentration of bigger particles is higher (7–18 nm) than before used under reaction (Fig. 8). This would assert that some sinterization process hardly occurs.

The inter-planar distance of the support was also measured resulting 1.2 nm in the fresh catalyst and 1.4 nm in the used. There is no evidence of structure damage after reaction.

EDX analysis on the LaInHM-f and LaInHM-u solids were performed (Fig. 9). The main observed difference is that after reaction the In and La particles are closer than in the fresh catalysts. In fact on the fresh catalyst several zones were scanned in order to determine the presence of both elements in the same area, but it was not feasible. However, in the used catalyst it was possible to find both types of particles together in several scanned areas (Fig. 9).

6. Main experimental evidence and conclusions

The maximum conversion of InHM and LaInHM in dry reaction conditions resulted 75% at 400 °C for InHM and 48% at 450 °C for the LaInHM sample.

From the catalytic activity results it could be concluded that the hydrothermal stability of the InHM catalysts is higher than in LaInHM solids. This conclusion does not agree with the results reported by Gutierrez and Lombardo [8]. They observed that the presence of lanthanum in the CoHM solid improves the hydrothermal stability of CoMordenite catalysts. This difference between LaInHM and CoLaHM may be due to the exchange process. In fact divalent cobalt ions are smaller than the trivalent indium, so the incorporation of lanthanum after the indium exchange should be more difficult than the addition of lanthanum into the CoHM. This factor conduces to lanthanum and indium species located in more external positions than the cobalt and lanthanum in the CoLaHM.

These authors concluded that lanthanum avoid the formation of EFAls species into the matrix of the CoLaHM catalyst. This effect seems to be the same in the LaInHM. In fact the EFALs sites do not increase after reaction on the LaInHM, while in the InHM-u the band at 3660 cm^{-1} in the FTIR spectra increases significantly. On the contrary, in the LaInHM catalysts the pore volume and the specific area decreased after reaction. This result support the hypothesis that lanthanum ions are not placed into internal positions, where the structure protection of lanthanum is only on the zeolite surface.

The hydrothermal treatment of **InHM** catalysts conduce to:

- Dealumination process (XPS, FTIR, XRD, N_2 adsorption)
- Decrease of total acidity (Py-TPD)
- Increment of the acidic strength (CO-TPD)
- Some slight sintering process (TEM)

The hydrothermal treatment of **LaInHM** catalysts conduce to:

- Slight dealumination process (XPS, FTIR)
- Decrease of total acidity (Py-TPD)
- Increment of the acidic strength (CO-TPD)
- Loss of specific area and pore volume (N_2 adsorption)
- Minor distance between the La and In particles, i.e. mobilization of particles during the reaction.

Finally, we could reach the following conclusions:

The comparison between InHM and LaInHM after reaction conduces to speculate that the exchanged lanthanum into the InHM catalyst protects the structure from the dealumination process. But the presence of this rare earth leads to a particular interaction with the indium active sites that would not improve the activity. This hypothesis is clearly evidenced by the XPS results where the concentration of $(InO)^+$ in LaInHM is lower than in the InHM catalyst. The last fact that cooperates with the LaInHM lower activity is the obstruction of mordenite channels due to the complex ion exchange process.

Acknowledgments

The authors wish to acknowledge the financial support received from ANPCyT, CONICET and UNL. Thanks are also given to Guillermina Amrein for the English language editing. Esteban Gioria and Santiago Ibarlín also want to thank to the Santa Fe Bank Foundation for the partial financing of this work within the student grant "Technological Innovation 2014".

Appendix A. Supplementary data

Supplementary data related to this article can be found at http://dx.doi.org/10.1016/j.micromeso.2015.09.042.

References

[1] W. Lutz, H. Toufar, R. Kurzhals, M. Suckow, Adsorption 11 (2005) 405–413.
[2] C.H. Bartholomew, Appl. Catal. A Gen. 212 (2001) 17–60.
[3] J.Z. Pieterse, R.W. Van den Brink, S. Booneveld, F. De Bruijin, Appl. Catal. B Env. 46 (2003) 239–250.
[4] P. Budi, R.F. Howe, Catal. Today 38 (1997) 175–179.
[5] A. Boix, E. Miró, E.A. Lombardo, M. Bañares, R. Mariscal, J.L.G. Fierro, J. Catal. 217 (2003) 186–194.
[6] P. Praserthdam, N. Mongkolsiri, P. Kanchanawanchkun, Catal. Comm. 3 (2002) 191–197.
[7] M.A. Ulla, L. Gutierrez, E.A. Lombardo, F. Lónyi, J. Valyon, Appl. Catal. A Gen. 277 (2004) 227–237.
[8] L. Gutierrez, E.A. Lombardo, Appl. Catal. A Gen. 360 (2009) 107–119.
[9] L. Gutierrez, A. Boix, E.A. Lombardo, J.L.G. Fierro, J. Catal. 199 (2001) 60–72.
[10] M. Ogura, S. Koge, M. Hayashi, M. Matsukata, E. Kikuchi, Appl. Catal. B Env. (2000) L213.
[11] F. Bustamante, F. Córdoba, M. Yates, C. Montes, Appl. Catal. A Gen. 234 (2002) 127–136.
[12] L. Gutierrez, A. Boix, J.O. Petunchi, J. Catal. 179 (1998) 179–191.
[13] L. Gutierrez, A. Boix, J.O. Petunchi, Catal. Today 54 (1999) 451–464.
[14] L.F. Córdoba, G.A. Fuentes, C. Montes de Correa, Microp. Mesop. Mat. 77 (2005) 193–201.
[15] L. Gutierrez, L. Cornaglia, E. Miró, J. Petunchi, Stud. Surf. Sc. Catal. 130 (2000) 1535–1540.
[16] E. Falabella Sousa-Aguiar, V.L. Doria Camorim, F.M. Zanon Zotin, R.L. Correa dos Santos, Microp. Mesop. Mat. 25 (1998) 25–34.
[17] E. Falabella Sousa-Aguiar, F.E. Trigueiro, F.M. Zanon Zotin, Catal. Today 218–219 (2013) 115–122.
[18] J.R. Bartlett, R.P. Cooney, R.A. Kydd, J. Catal. 114 (1988) 53–57.
[19] J.G. Kim, T. Kompany, R. Ryoo, T. Ito, J. Fraissard, Zeolites 14 (1994) 427–432.
[20] J.G. Nery, Y. Mascarenhas, T.J. Bonagamba, N. Mello, E. Falabella, S. Aguiar, Zeolites 18 (1997) 44–49.
[21] E.F.T. Lee, L.V.C. Rees, Zeolites 7 (1987) 446–450.
[22] R. Carvajal, P. Chee, J.H. Lunsford, J. Catal. 125 (1990) 123–131.
[23] F. Lemos, F.R. Ribeiro, M. Kern, G. Giannetto, M. Guisnet, Appl. Catal. 39 (1988) 227–237.
[24] G. Yang, Y. Wang, D. Zhou, J. Zhuang, X. Liu, X. Han, X. Bao, J. Chem. Phys. 119 (18) (2003) 9765–9770.
[25] G. Yang, J. Zhuang, Y. Wang, D. Zhou, M. Yang, X. Liu, X. Han, X. Bao, J. Molec. Struc. 737 (2005) 271–276.
[26] G. Yang, Y. Wang, D. Zhou, X. Liu, X. Han, X. Bao, J. Mol. Catal. A Chem. 237 (2005) 36–44.
[27] T. Maunula, J. Ahola, H. Hamada, Appl. Catal. B Env. 64 (2006) 13–24.
[28] E.M. Sadovskaya, A.P. Suknev, L.G. Pinaeva, V.B. Goncharov, B.S. Bal'zhinimaev, C. Chupin, J. Pérez-Ramírez, C. Mirodatos, J. Catal. 225 (2004) 179–189.
[29] X. She, M. Flytzani-Stephanopoulos, J. Catal. 237 (2006) 79–93.
[30] T. Sowade, C. Schmidt, F.-W. Schütze, H. Berndt, W. Grünert, J. Catal. 214 (2003) 100–112.
[31] E. Kikuchi, M. Ogura, Catal. Surv. Jpn. 1 (1997) 227–237.
[32] Y. Ogura, Y. Sugiura, M. Hayashi, E. Kikuchi, Catal. Lett. 42 (1996) 185–189.
[33] J.M. Ramallo-López, L.B. Gutierrez, A.G. Bibiloni, F.G. Requejo, E.E. Miró, Catal. Lett. 82 (1–2) (2002) 131–139.
[34] C. Schmidt, Thomas Sowade, Elke Löffler, A. Birkner, W. Grünert, J. Phys. Chem. B 106 (2002) 4085–4097.
[35] J.M. Ramallo-López, F.G. Requejo, L.B. Gutierrez, E.E. Miró, Appl. Catal. B Env. 29 (2001) 35–46.
[36] L. Gutierrez, A. Boix, H. Decolatti, H. Solt, F. Lonyi, E. Miró, Microp. Mesop. Mat. 163 (15) (2012) 307–320.
[37] F. Lonyi, H. Solt, J. Valyon, J. Valyon, H. Decolatti, L. Guierrez, E. Miró, Appl. Catal. B Env. 100 (2010) 133–142.
[38] F. Lonyi, H. Solt, J. Valyon, J. Valyon, A. Boix, L. Guierrez, J. Molec. Catal. A Chem. 345 (2011) 75–80.
[39] J.M. Ramallo, A. Bibiloni, F. Requejo, L. Gutierrez, E. Miró, J. Phys. Chem. B 106 (2002) 7815–7823.
[40] L. Gutierrez, J.M. Ramallo López, S. Irusta, E. Miró, F.G. Requejo, J. Phys. Chem. B 105 (2001) 9514–9523.
[41] L. Gutierrez, M.A. Ulla, E. Lombardo, A. Kovács, F. Lónyi, J. Valyon, Appl. Catal. A Gen. 292 (2005) 154–161.
[42] J.M. Zamaro, E. Miró, A.V. Boix, A. Martínez-Hernández, G. Fuentes, Microp. Mesop. Mater. 129 (2010) 74–81.
[43] A. Gabrienko, S.S. Arzumanov, I.B. Moroz, I.P. Prosvirin, A.V. Toktarev, W. Wang, A.G. Stepanov, J. Phys. Chem. C 118 (2014) 8034–8043.
[44] R.M. Mihályi, Z. Schay, Á. Szegedi, Catal. Today 143 (2009) 253–260.
[45] T. Zhang, F. Gu, D. Han, Z. Wang, G. Guo, Sensors Actuators B Chem. 177 (2013) 1180–1188.
[46] W. Grünert, U. Sauerlandt, R. Schlögl, H.G. Karge, J. Phys. Chem. 97 (1993) 1413–1419.
[47] Y. Cheng, J. Hoard, C. Lambert, J.H. Kwak, C.H.F. Peden, Catal. Today 136 (2008) 34–39.
[48] P.N.R. Vennestrøm, T.V.W. Janssens, A. Kustov, M. Grill, A. Puig-Molina, L.F. Lundegaard, R.R. Tiruvalam, P. Concepción, A. Corma, J. Catal. 309 (2014) 477–490.
[49] R.W. Hartford, M. Kojima, C.T. O'Connor, Ind. Eng. Chem. Res. 28 (1989) 1748–1752.
[50] C.R. Moreira, N. Horms, J.L.G. Fierro, M.M. Pereira, P.R. de la Piscina, Microp. Mesop. Mater. 133 (2010) 75–81.
[51] R. Dimitijevic, J. Phys. Chem Solids 67 (2006) 1741–1748.
[52] E. Selli, L. Forni, Microp. Mesop. Mater. 31 (1999) 129–140.
[53] E. Finocchio, T. Montanari, C. Resini, G. Busca, J. Mol. Catal. A Chem. 204–205 (2003) 535–544.
[54] C. Pazé, S. Bordiga, C. Lamberti, M. Salvalaggio, A. Zecchina, J. Phys. Chem. B 101 (1997) 4740–4751.
[55] M.C. Campa, I. Luisetto, D. Pietrogiacomi, V. Indovina, Appl. Catal. B Env. 46 (2003) 511–522.
[56] E. Bourgeat-Lami, P. Massiani, F. Di Renzo, P. Espiau, P. Fajula, Appl. Catal. 72 (1991) 139–152.
[57] I. Kiricsi, C. Flego, G. Pazzucconi, W.O. Parker, R. Millini, C. Perego, G.J. Bellusi, J. Phys. Chem. 98 (1994) 4627–4634.
[58] A. Zecchina, S. Bordiga, G. Spoto, D. Scarano, G. Petrini, G. Leofanti, M. Padovan, C. Otero Areàn, J. Chem. Soc. Faraday Trans. 88 (1992) 2959–2969.
[59] T. Montanari, E. Finocchio, G. Busca, J. Phys. Chem. C 115 (2011) 937–943.
[60] J. Datka, B. Gil, A. Kubacka, Zeolite 15 (1995) 501–516.
[61] P. Tynjala, J. Molec. Catal. A Chem. 110 (1996) 153–161.
[62] A. Zecchina, L. Marchese, S. Bordiga, C. Pazè, E. Gianotti, J. Phys. Chem. B 101 (48) (1997) 10128–10135.
[63] C.O. Areán, T. Palomino, F. Geobaldo, A. Zecchina, J. Phys. Chem. 100 (1996) 6689.
[64] S. Bordiga, C. Lamberti, G. Geobaldo, A. Zecchina, Langmuir 11 (1995) 527–533.
[65] V. Mavrodinova, M. Popova, M.R. Mihály, G. Pál-Borbély, C. Minchev, Appl. Catal. A Gen. 262 (2004) 75–83.
[66] T. Bučko, J. Hafner, L. Benco, J. Phys. Chem. B 109 (2005) 7345–7357.
[67] L. Kubelková, S. Beran, J.A. Lercher, Zeolites 9 (1989) 539–543.
[68] S. Kotrel, J.H. Lunsford, H. Knözinger, J. Phys. Chem. B 105 (2001) 3917–3921.